

Formation of Island SERS Films on Surfaces of Track Membranes and Silicon Substrates

S. I. Serebrennikova^a, V. I. Kukushkin^{b, *}, O. V. Kristavchuk^c, E. N. Morozova^b,
A. S. Astrakhantseva^{b, d}, and A. N. Nechaev^c

^a Skolkovo Institute of Science and Technology, Moscow, 121205 Russia

^b Institute of Solid State Physics, Russian Academy of Sciences, Chernogolovka, Moscow oblast, 142432 Russia

^c Joint Institute for Nuclear Research, Dubna, Moscow oblast, 141980 Russia

^d Moscow Institute of Physics and Technology, Dolgoprudny, Moscow oblast, 141701 Russia

*e-mail: kukushvi@mail.ru

Received November 15, 2021; revised December 6, 2021; accepted December 22, 2021

Abstract—It is shown that metallic nano-island SERS-active layers can be created on the surfaces of porous track membranes made of polyethylene terephthalate and silicon substrates optimized for exciting laser radiation with wavelengths of 532 and 785 nm. Characteristic patterns of changes in the optical properties of SERS structures upon altering the morphology of metal nanoparticles on a substrate's surface are established. Such structures can be used as SERS chips and highly sensitive filtering SERS elements in optical biosensors.

DOI: 10.3103/S1062873822040207

INTRODUCTION

Creating biosensors for highly sensitive screening and detection of infectious diseases is one of the most important problems of the scientific community, especially during the ongoing COVID-19 pandemic. Promising ways of detecting biological targets are ones based on optical spectroscopy [1, 2]. Technologies based on surface-enhanced Raman scattering (SERS) spectroscopy are of particular interest in solving this problem, due to their high sensitivity and operating speed [3–8]. However, when using the conventional “sandwich” approach [9] to improve contrast in the SERS signal between a test specimen (which contains a given biological target) and a control specimen (without a target), we must classify a sample to distinguish it from proteins and randomly deposited reporter molecules. There are many ways of classifying a sample (e.g., according to mass, size, elasticity, and electrical and magnetic properties).

In this work, we demonstrate the possibility of creating optical sensors based on track membranes (TMs) made of polyethylene terephthalate (PET). These sensors have SERS-active surfaces and serve as filtering elements. A track membrane is a convenient substrate for forming a nano-structured layer, since it has a smooth surface. The use of such membranes as flow sensors offers advantages typical of this type of membranes. The diameter of TM pores varies over a wide range, from 10 nm to 7 μm ; their surface density, from 10^5 to 10^9 cm^{-2} . The geometric parameters of the pore

channels can be changed. TMs have good mechanical characteristics, since the material they are made of is biologically inert. In [10], we described a procedure for creating SERS structures on the surface of a TM (made of PET) from colloid nanoparticles of silver obtained using electric-spark discharges in water.

The aim of this work was to compare the geometrical parameters and optical properties of island nanostructures obtained on porous and nonporous polymer and silicon substrates. Vacuum thermal deposition with computer-aided control of the width and rate of deposition was used to create island metal nanolayers.

EXPERIMENTAL

To study the effect the morphology of metal nanoparticles has on the optical properties of SERS structures, we created SERS films on the surfaces of Si/SiO₂ substrates, track membranes made of PET, and nonporous films also made of PET.

The track membranes were obtained at the Joint Institute for Nuclear Research's Flerov Laboratory of Nuclear Reactions, using the technology described in [11]. The procedure for obtaining track membranes is based on interaction between beams of accelerated heavy ions and a polymer. As they pass through a polymer film, multiply charged high-energy ions leave zones of destruction along the trajectories (tracks) of bombarding particles. The irradiated film is then additionally subjected to photooxidation using ultraviolet

(UV) radiation, allowing more selective disintegration of the destroyed regions inside the polymer via chemical etching (with alkaline solutions for PET) [12]. The TM used in this work was made of a PET film (Hostaphan RNK, Mitsubishi Polyester) 19 μm thick. The film was irradiated on an ITs-100 accelerator by beams of Xe^{26} ions with energies of 1.16–1.22 MeV/n. Chemical etching was done with 2.2 M of NaOH solution at a temperature of 85°C. The average diameter of pores on the surface was 0.36 μm , and the pore density was $2.6 \times 10^8 \text{ cm}^{-2}$.

Thin metal layers were deposited onto the substrate's surface using a NANO 38 system of vacuum thermal deposition (Kurt J. Lesker Co., United States) with computer-aided control of their thickness at a pressure of 8×10^{-7} torr in the chamber with a 0.4 $\text{\AA}/\text{s}$ rate of deposition. The substrates were then heated on an HP-20D-Set hotplate (Daihan Scientific, South Korea), and SERS surfaces formed with a variety of lateral sizes, heights, shapes, and gaps between metal nanoparticles.

According to data obtained in [13], nominal thickness h of deposited silver was varied from 6 to 30 nm (6, 10, 15, 20, 25, and 30 nm) to optimize the island SERS films on Si/SiO₂ substrates (the layer of silicon oxide was 300 nm thick). The nominal thickness of gold was varied from 4.5 to 25 nm (4.5, 10, 15, 20, and 25 nm). After deposition, the specimens were annealed on the heating plate for 6 min each at $T = 120, 240, \text{ and } 360^\circ\text{C}$, respectively. Specimens with no annealing were investigated as well.

The layers of silver deposited onto the films and TMs made of PET were 6, 10, 15, and 20 nm thick. After deposition, the specimens were annealed for 6 min each at $T = 120, 160, \text{ and } 200^\circ\text{C}$, respectively. Subsequent increases in temperature were limited by the thermal stability of the polymer ($\sim 250^\circ\text{C}$). The obtained specimens were compared to those not subjected to annealing.

EnSpectr R532 (wavelength of laser radiation, 532 nm; power, 30 mWt; spectral resolution, 4–6 cm^{-1}) and EnSpectr R785 (wavelength of laser radiation, 785 nm; power, 50 mWt; spectral resolution, 6–8 cm^{-1}) Raman spectrometers (RamMiks, Russia) based on the ADF U300 optical microscope (ADF Optics Ltd., China) were used to measure the SERS signal from test molecules of 4-ABT (4-Aminobenzenethiol; CAS no. 1193-02-8; Sigma-Aldrich, United States). All measurements were made with a 10 \times objective and repeated ten times. The resulting spectra were averaged.

The morphology of the surfaces of SERS substrates based on Si/SiO₂ was studied via SEM using a Supra 50VP electron microscope (Zeiss, Germany) with a superhigh resolution of 1.5 nm. The specimens based on PET films and track membranes were studied on a high-resolution SU8020 microscope (Hitachi, Japan)

using a cold field emission cathode with a preliminarily deposited thin conducting layer of PtPd alloy.

The images of specimens were processed with the Scanning Probe Image Processor (SPIP) program to determine the sizes of silver and gold nanoparticles deposited onto silicon substrates. This program allowed us to recognize objects in an image with luminance higher than the threshold value, which was set manually for each image. The program automatically calculated the area of recognized objects. The data on the diameters and areas of the particles obtained in SPIP were used in the Origin program, with which the diameter distributions in each image were constructed. Since the shape of the obtained distributions (except for thick films with a high degree of coverage) was close to Gaussian, they were approximated with the tools of the Origin program using the Gaussian

$$\text{function } y = y_0 + \frac{A}{\sigma\sqrt{\pi/4 \ln 2}} \exp\left(-4 \ln 2 \frac{(d - d_a)^2}{\sigma^2}\right).$$

The values of the average diameter d_a and dispersion σ were calculated automatically by this program, along with their errors.

SEM images of the specimens made of PET were not processed with the SPIP program because the contrast in the obtained images was poor, due to the conditions of acquiring images on the surfaces of track membranes. PET is destroyed under the action of electron beams with energies higher than 3 keV, which determines the low resolution of the electron microscope. As a result, the contrast in the images did not meet the conditions for processing in the SPIP program.

RESULTS AND DISCUSSION

In this work, we investigated dependences of the intensity of SERS line 1140 cm^{-1} of the test substance 4-ABT on the average lateral sizes and shapes of nanoparticles and the gaps between them.

Tables 1–3 present data on the intensities of SERS, depending on the morphology of nanoparticles (average diameter d_a , diameter dispersion σ , coefficient of surface filling with metal nanoparticles S) for each mode of substrate annealing t after deposition and for each thickness h of the deposited metal layers. Table 1 presents data from depositing silver onto an Si/SiO₂ substrate; Table 2, from depositing gold onto a Si/SiO₂ substrate; and Table 3, for depositing silver onto the surfaces of PET films.

The patterns described below were established by studying the effect the morphology of metal nanoparticles had on the SERS signals from Si/SiO₂ substrates during excitation by laser radiation with wavelengths of 532 and 785 nm. When using thick (10 to 25 nm) deposited layers of silver or gold with no thermal annealing, prolate nanostructures with high coefficients of filling S (Table 1 and 2) formed on the sur-

Table 1. Dependence of SERS intensity on the morphology of nanoparticles of silver on the surface of Si/SiO₂ substrates in different modes of deposition and annealing

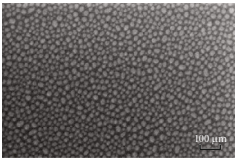
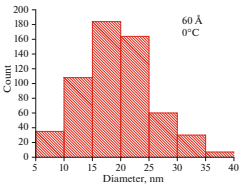
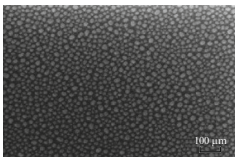
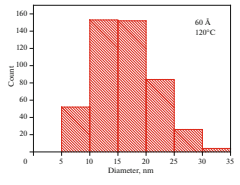
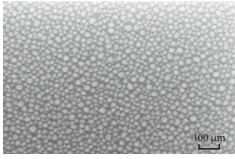
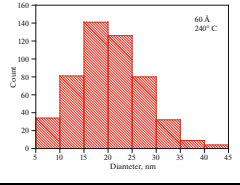
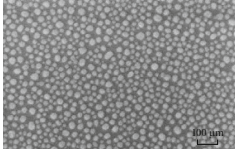
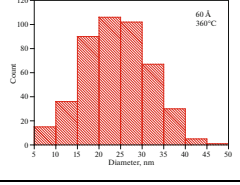
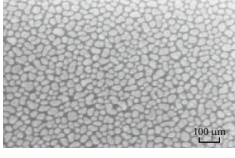
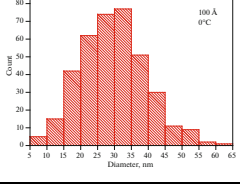
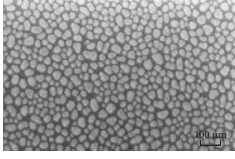
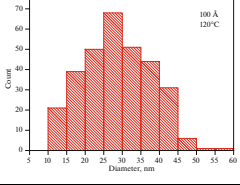
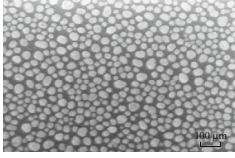
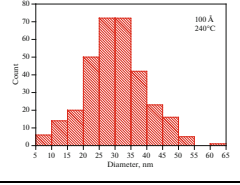
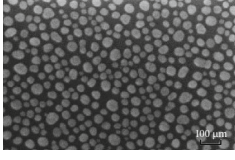
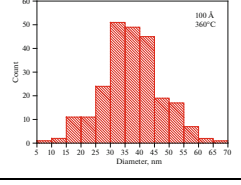
h , nm	T , °C	S , %	d_a , nm	σ , nm	SERS $\lambda = 532$ nm, rel. units	SERS $\lambda = 785$ nm, rel. units	SEM images	Histogram
6	25	44	19	13.9	56600	550		
6	120	39	16	13.3	50600	420		
6	240	47	20	16.6	75020	420		
6	360	46	24	19.6	60400	920		
10	25	55	29	22.3	32440	20800		
10	120	47	28	26.3	91570	2020		
10	240	47	30	18.2	96640	1020		
10	360	45	37	19.1	59360	1550		

Table 1. (Contd.)

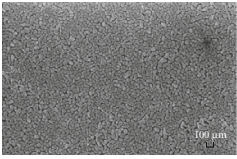
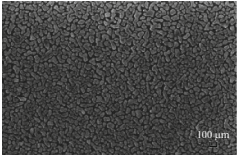
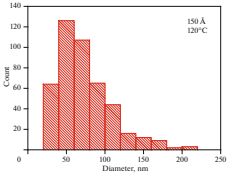
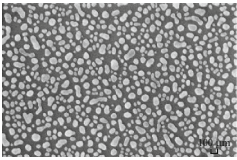
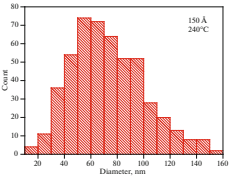
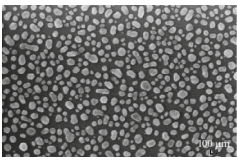
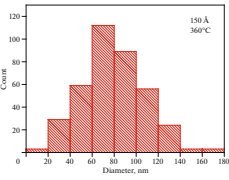
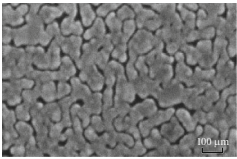
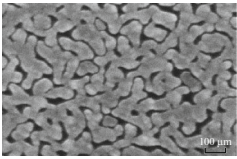
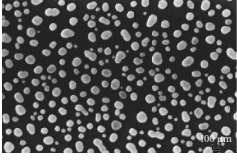
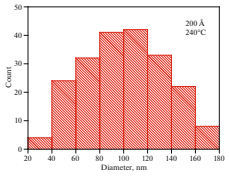
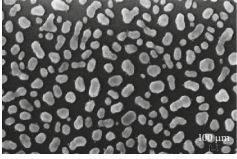
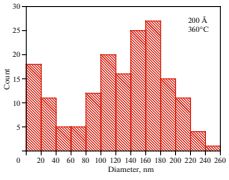
h , nm	T , °C	S , %	d_a , nm	σ , nm	SERS $\lambda = 532$ nm, rel. units	SERS $\lambda = 785$ nm, rel. units	SEM images	Histogram
15	25	66	—	—	46840	36400		—
15	120	60	61	60.7	58000	26870		
15	240	43	68	61	30470	1025		
15	360	40	78	65.2	11800	1525		
20	25	88	—	—	15200	39240		—
20	120	85	—	—	34685	8260		—
20	240	31	101	119	3600	130		
20	360	40	149	113.5	4420	550		

Table 1. (Contd.)

h , nm	T , °C	S , %	d_a , nm	σ , nm	SERS $\lambda = 532$ nm, rel. units	SERS $\lambda = 785$ nm, rel. units	SEM images	Histogram
25	25	81	—	—	7750	32660		—
25	120	26	9	6	3500	7820		
25	240	46	183	133	1255	250		
25	360	38	192	118	595	150		
30	25	86	—	—	820	1070		—
30	120	45	19	11	1270	170		
30	240	53	—	—	2010	180		—
30	360	35	334	244	400	140		

Table 2. Dependence of SERS intensity on the morphology of nanoparticles of gold on the surfaces of Si/SiO₂ substrates in different modes of deposition and annealing

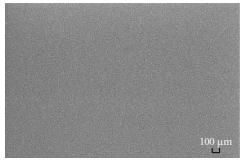
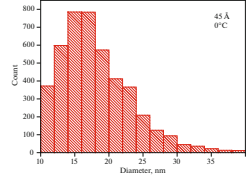
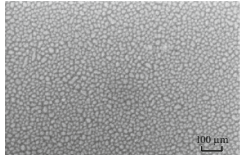
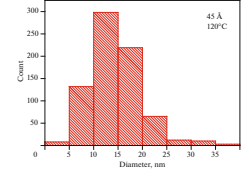
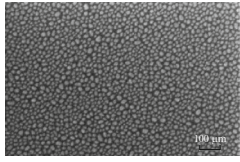
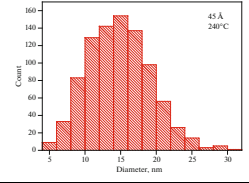
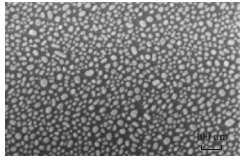
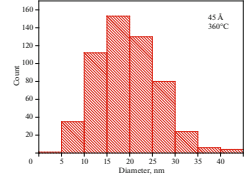
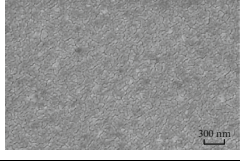
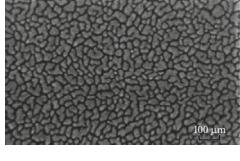
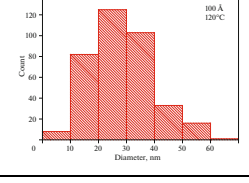
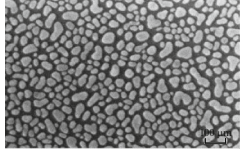
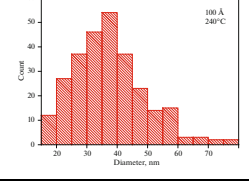
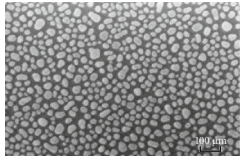
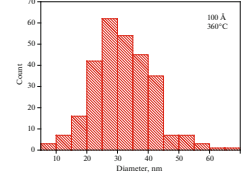
h , nm	T , °C	S , %	d_a , nm	σ , nm	SERS $\lambda = 532$ nm, rel. units	SERS $\lambda = 785$ nm, rel. units	SEM image	Histogram
4.5	25	42	16	11.5	476	760		
4.5	120	38	14	11	1120	475		
4.5	240	31	14	10.7	1222	320		
4.5	360	38	19	16.8	1206	295		
10	25	67	—	—	406	3572		—
10	120	43	27	26.2	630	2874		
10	240	52	35	24	1210	597		
10	360	51	31	21.4	855	288		

Table 2. (Contd.)

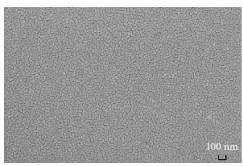
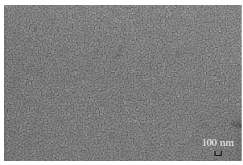
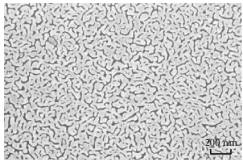
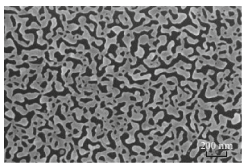
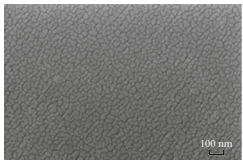
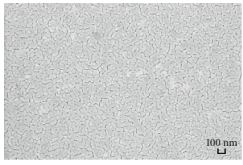
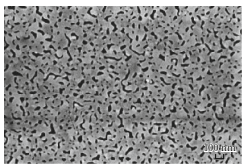
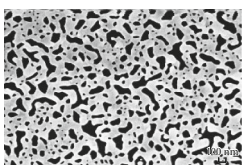
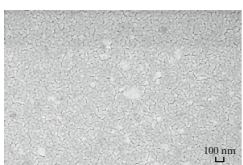
h , nm	T , °C	S , %	d_a , nm	σ , nm	SERS $\lambda = 532$ nm, rel. units	SERS $\lambda = 785$ nm, rel. units	SEM image	Histogram
15	25	76	—	—	578	6800		—
15	120	76	—	—	355	7160		—
15	240	82	—	—	404	522		—
15	360	57	—	—	350	340		—
20	25	95	—	—	380	5640		—
20	120	92	—	—	280	3624		—
20	240	79	—	—	353	505		—
20	360	70	—	—	400	250		—
25	25	96	—	—	230	2950		—

Table 2. (Contd.)

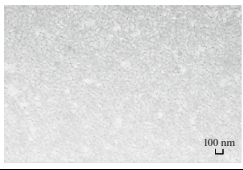
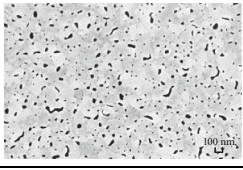
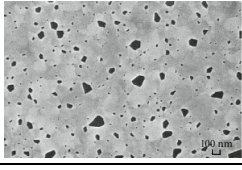
h , nm	T , °C	S , %	d_a , nm	σ , nm	SERS $\lambda = 532$ nm, rel. units	SERS $\lambda = 785$ nm, rel. units	SEM image	Histogram
25	120	98	—	—	198	1634		—
25	240	93	—	—	270	250		—
25	360	93	—	—	205	250		—

Table 3. Dependence of SERS intensity on the morphology of nanoparticles of silver on the surfaces of PET substrates in different modes of deposition and annealing

Modes	Thickness of Ag			
	6 nm	10 nm	15 nm	20 nm
Without heating (25°C)	365	708	772	322
120°C	8740	4120	3054	1308
160°C	6265	1940	940	734
200°C	1230	1294	1140	985

faces of silicon substrates. They had a maximum of plasmon absorption in the near IR region [14] and a high coefficient of Raman scattering amplification at a laser excitation wavelength of 785 nm.

Upon laser excitation with a wavelength of 532 nm, the increase in the optical response from the test substance at an Ag/SiO₂ interface was two orders of magnitude higher than the one in the signal at an Au/SiO₂ interface. Upon laser excitation with a wavelength of 785 nm, the increase in the signal was 3–5 times greater (depending on the mode of thermal annealing) at an Ag/SiO₂ interface than at an Au/SiO₂ interface (Fig. 1). The smaller increase in the signal from gold is explained by an increase in the imaginary part of permittivity created by interband transitions being observed in the metal's range of optical frequencies [15]. This is one reason for the damping of surface plasmon polaritons. The equalization of coefficients of amplification in the IR region was due to the shift of

the position (upon moving from Ag/SiO₂ to Au/SiO₂) of the plasmon absorption contour to the red region of the spectrum [16].

- For silver layers 6 and 10 nm thick, the percentage of filling and shape (round) were approximately the same at all temperatures of annealing. With silver layers 15 and 20 nm thick, the percentage of filling at temperatures of annealing 0 and 120°C was much higher than when heated to temperatures of 240 and 360°C. For thicknesses of 25 and 30 nm with no heating, the percentage of the surface filled with metal was considerably higher than with heating. The average diameters of particles with identical modes of annealing grew along with the thickness of the silver layer.

- For gold layers 4.5 and 10 nm thick, the percentages of filling were moderate for all temperatures of annealing and took values of 31 to 52%. With gold layers thicker than 10 nm, nanogranules started to

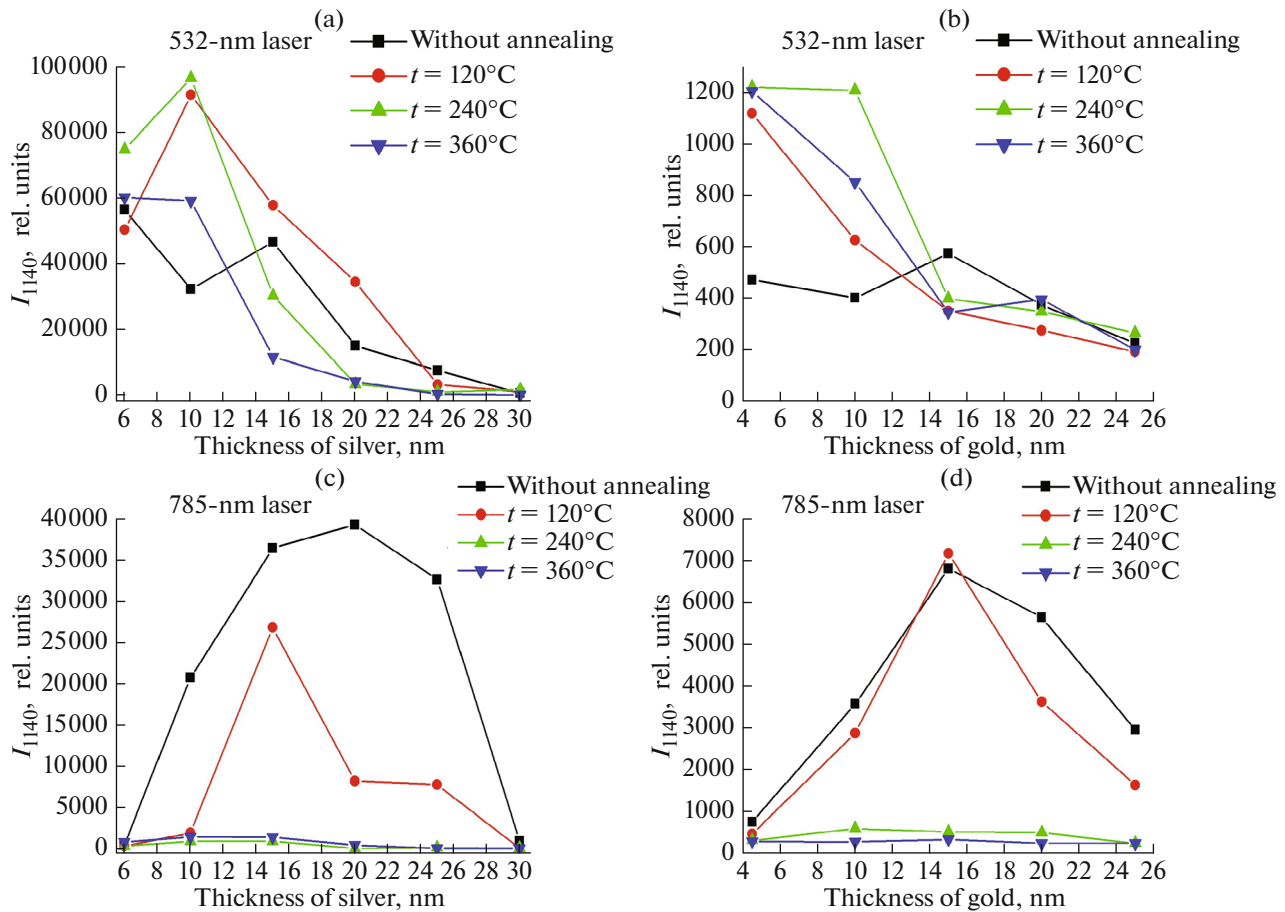


Fig. 1. Dependences of the intensity of SERS lines 1140 cm^{-1} of the 4-ABT on the thickness of metal deposited onto Si/SiO₂ substrates in different modes of annealing: (a) for silver upon excitation by laser radiation with a wavelength of 532 nm; (b) for gold upon excitation by laser radiation with a wavelength of 532 nm; (c) for silver upon excitation by laser radiation with a wavelength of 785 nm; (d) for gold upon excitation by laser radiation with a wavelength of 785 nm.

stick together and the percentage of filling grew considerably.

- When gold and silver SERS substrates were heated by laser radiation with a wavelength of 532 nm, the intensity of Raman scattering mainly fell as the deposited layer grew thicker in all modes of heating (and with no heating) (Figs. 1a, 1b). Such behavior differs considerably from the results of measurements obtained using probe radiation with a wavelength of 785 nm (Figs. 1c, 1d). Intensity was virtually independent of the thickness of the deposited film at high temperatures of heating (240 and 360°C) for both silver and gold substrates. With weak and no heating, however, the intensity of Raman scattering grows sharply by two orders of magnitude for deposited silver layers 10 to 25 nm thick, and by one order of magnitude for gold layers 10 to 20 nm thick.

- SERS substrates with layers of silver 10 nm thick and annealed at a temperature of 120°C exhibited the highest coefficient of Raman scattering amplification at a 532 nm wavelength of probe laser radiation

(Table 1). SERS substrates with layers of silver 20 nm thick and no thermal treatment exhibited the highest coefficient of Raman scattering amplification at a 785 nm wavelength of probe laser radiation (Table 1).

When the thickness of a silver layer deposited on a polymer surface is raised, nanospheres grow until they coalesce and lateral wavy structures form. No appreciable differences (effects of pores) are observed in silver layers obtained on nonporous and porous surfaces. The size of the nanospheres grows slightly due to their coalescence and the enlargement of lateral structures when the temperature of annealing is raised on specimens with identical thicknesses of deposited layers (Figs. 2, 3). Amplification of the signal of Raman scattering on PET reaches its maximum value with silver layers 6 nm thick and annealing at a temperature of 120°C (Fig. 4). As the thickness of silver layers and the temperature of annealing grow, the intensity of SERS signals falls drastically. Depositing a silver layer thicker than 6 nm covers the polymer surface of a film or track membrane completely. On PET substrates with no

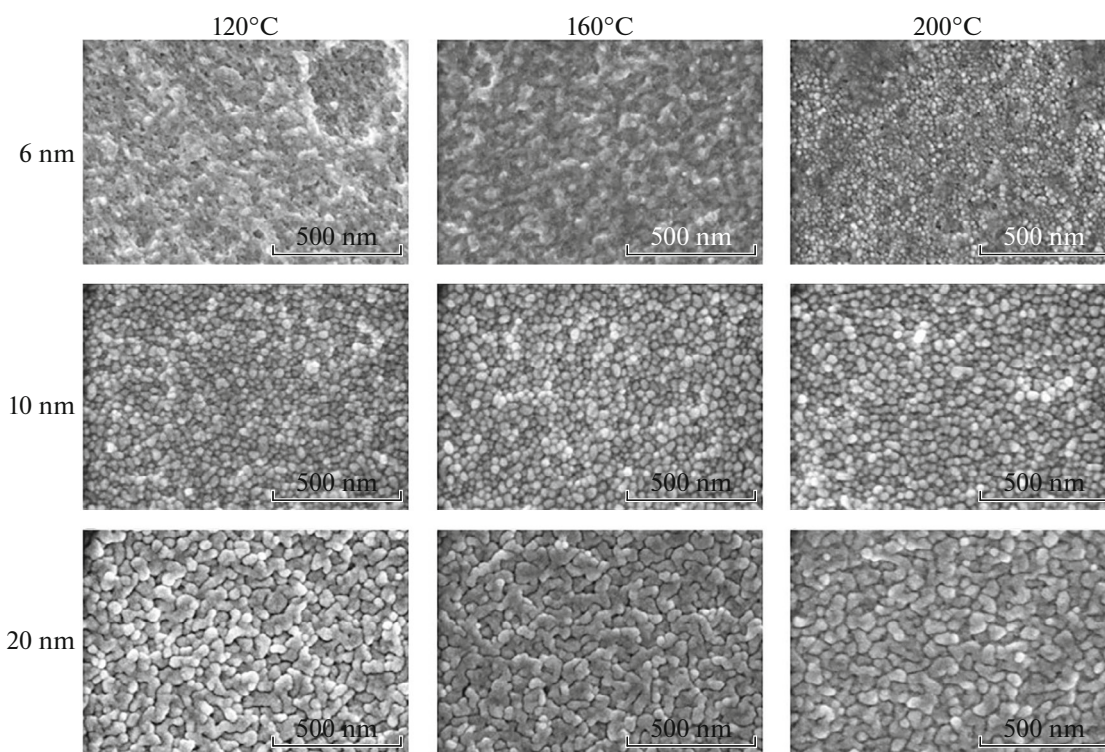


Fig. 2. SEM of PET films with different thicknesses of a deposited layer of silver at different temperatures of annealing.

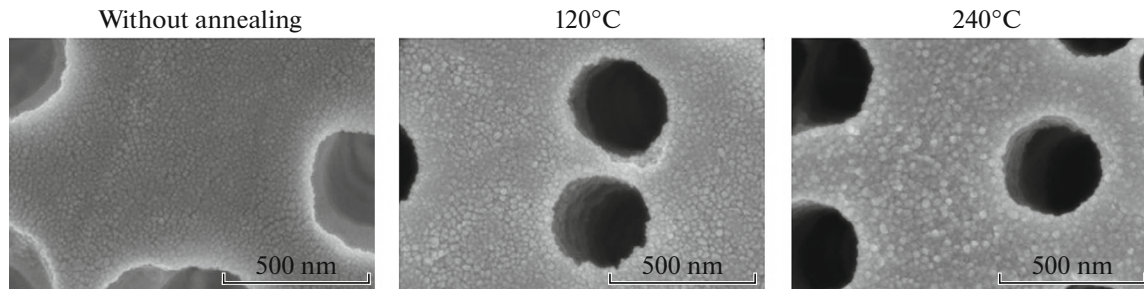


Fig. 3. SEM of PET TMs with layers of silver 6 nm thick at different temperatures of annealing.

thermal impact or a powerful thermal impact (200°C), the SERS signal is low at any silver layer thickness (Table 3). In the first case, this is because there are no pronounced nanospheres; in the second, it has to do with the formation of prolate nanostructures that provide plasmon resonance in the red spectral band (far from the frequency of laser excitation).

CONCLUSIONS

In metal nanoparticles whose sizes are comparable to the depth of penetration of the electromagnetic field of visible laser radiation (10–50 nm), the properties of surface plasmon polaritons depend strongly on the geometric sizes of the former [13]. It was shown that

upon laser excitation with a wavelength of 532 nm, the best SERS nanostructures are surfaces in the shape of round metal granules with an ~50% coefficient of filling; at a wavelength of 785 nm, they are in the shape of prolate granules with coefficients of filling greater than 75% (Tables 1 and 2). Patterns of changes in the optical properties of silver and gold SERS substrates based on Si/SiO₂ upon altering the morphology of metal nanoparticles were established by means of Raman spectroscopy.

Similar conditions were applied to form SERS-active layers on the surfaces of polymer films and track membranes made of polyethylene terephthalate. It was shown that the maximum intensity of the signal is

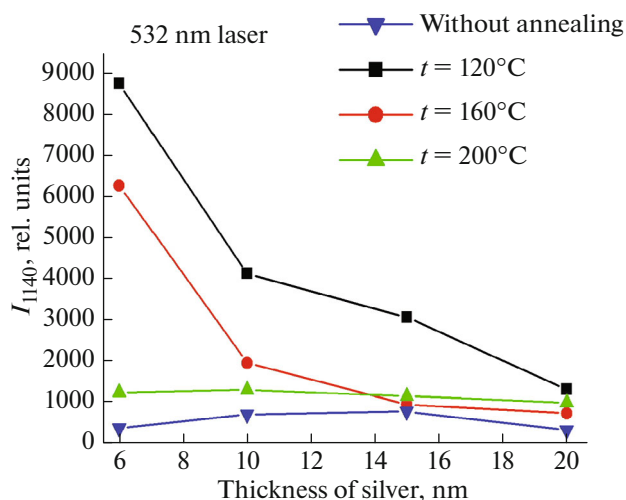


Fig. 4. Graphs of dependences of the intensity of SERS line 1140 cm^{-1} of 4-ABT on the thickness of a layer of silver deposited onto a PET substrate at different temperatures of annealing.

reached with silver nanostructure deposits 6 nm thick and an annealing temperature of 120°C . Our porous SERS-active substrates can be used for the preliminary purification of samples and subsequent detection via Raman spectroscopy.

These results are of considerable applied importance, since our highly sensitive optical sensors based on filtering elements in the shape of track membranes can be used in medicine, biology, industry, and agriculture.

ACKNOWLEDGMENTS

The authors thank the shared resource center of the Institute of Solid State Physics, Russian Academy of Sciences, for allowing us to use its scanning electron microscope in our investigations.

FUNDING

This work was supported by the Russian Foundation for Basic Research, project no. 20-04-60077.

CONFLICT OF INTEREST

The authors declare that they have no conflicts of interest.

REFERENCES

- Jin, C.J., Lee, T.Y., Koo, B., et al., *Sens. Actuators, B*, 2018, vol. 255, p. 2399.
- Maddali, H., Miles, C.E., Kohn, J., and O'Carroll, D.M., *ChemBioChem*, 2021, vol. 22, p. 1176.
- Sha, M.Y., Xu, H., Penn, S.G., et al., *Nanomedicine*, 2007, vol. 2, p. 725.
- Chon, H., Lee, S., Son, S.W., et al., *Anal. Chem.*, 2009, vol. 8, p. 3029.
- Wang, J., Wu, X., Wang, C., et al., *ACS Appl. Mater. Interfaces*, 2016, vol. 31.
- Lopez, A., Lovato, F., Oh, S.H., et al., *Talanta*, 2015, vol. 146, p. 388.
- Gribanyov, D., Zhdanov, G., Olenin, A., et al., *Int. J. Mol. Sci.*, 2021, vol. 22, p. 1842.
- Zavyalova, E., Ambartsumyan, O., Zhdanov, G., et al., *Nanomaterials*, 2021, vol. 11, p. 1394.
- Kukushkin, V.I., Ivanov, N.M., Novoseltseva, A.A., et al., *PLoS One*, 2019, vol. 14, e0216247.
- Kristavchuk, O.V., Nikiforov, I.V., Kukushkin, V.I., et al., *Colloid J.*, 2017, vol. 79, p. 637.
- Flerov, G.N., Apel', P.Yu., Didyk, A.Yu., et al., *At. Energ.*, 1989, vol. 67, no. 4, p. 274.
- Apel, P.Yu., *Radiat. Instrum.*, 1995, vol. 25, nos. 1–4, p. 667.
- Kukushkin, V.I., Astrakhantseva, A.S., and Morozova, E.N., *Bull. Russ. Acad. Sci.: Phys.*, 2021, vol. 85, p. 133.
- Huang, X., Neretina, S., and El-Sayed, M.A., *Adv. Mater.*, 2009, vol. 48, p. 4880.
- Johnson, P.B. and Christy, R.W., *Phys. Rev. B*, 1972, vol. 6, p. 4370.
- Garcia, M.A., *J. Phys. D: Appl. Phys.*, 2011, vol. 44, 283001.

Translated by E. Smirnova